

Article

TiO₂–Fe₃O₄ Composite Systems—Preparation, Physicochemical Characterization, and an Attempt to Explain the Limitations That Arise in Catalytic Applications

Rafal Krakowiak ^{1,*}, Robert Frankowski ², Kinga Mylkie ³, Dariusz T. Mlynarczyk ¹,
Marta Ziegler-Borowska ³, Agnieszka Zgoła-Grześkowiak ² and Tomasz Goslinski ^{1,*}

¹ Chair and Department of Chemical Technology of Drugs, Poznan University of Medical Sciences, Grunwaldzka 6, 60-780 Poznan, Poland

² Institute of Chemistry and Technical Electrochemistry, Poznan University of Technology, Berdychowo 4, 60-965 Poznan, Poland

³ Medicinal Chemistry Research Group, Department of Biomedical & Polymer Chemistry, Faculty of Chemistry, Nicolaus Copernicus University in Torun, Gagarina 7, 87-100 Torun, Poland

* Correspondence: rafal.krakowiak@student.ump.edu.pl (R.K.); tomasz.goslinski@ump.edu.pl (T.G.)

Abstract: In this work, a composite material based on titanium(IV) oxide and iron(II,III) oxide was prepared using mechanochemical method. The obtained composite system was thoroughly characterized using techniques such as scanning electron microscopy, X-ray powder diffraction, thermogravimetric analysis, and nanoparticle tracking analysis. The acute toxicity of the composite material was evaluated with Microtox. In addition, the material's photocatalytic potential was studied in photodegradation tests of ibuprofen. The composite system revealed magnetic properties of potential usage in its recovery after photocatalytic tests. However, the photocatalytic activity of TiO₂–Fe₃O₄ was lower than that of bare TiO₂. In the photocatalytic tests performed under UV (365 nm) light, a 44% reduction of initial ibuprofen concentration in the sample was noted for bare TiO₂, while for TiO₂–Fe₃O₄ composite, only a 19% reduction was observed. In visible light (525 nm), both materials achieved statistically insignificant photodegradation rates, which was contrary to the anticipated effect for TiO₂–Fe₃O₄. The observation was explained by a side oxidation reaction of Fe₃O₄ to Fe₂O₃ by the generated reactive oxygen species (ROS) in the photocatalytic process, which significantly diminished the amount of available ROS for ibuprofen degradation. The oxidation process appearing within TiO₂–Fe₃O₄ was evident and easily observed as the color of the material turned from gray to brown. Acute toxicity assay performed with the use of Microtox revealed reduced toxicity of TiO₂–Fe₃O₄ (32% inhibition of the *Aliivibrio fischeri* bacteria cell viability according to bioluminescence emitted) when compared to bare Fe₃O₄ (56% inhibition), whereas bare TiO₂ was non-toxic. In the study, the processes occurring during the photocatalytic reaction were analyzed and discussed in the context of the available literature data.

Keywords: titanium(IV) oxide; iron(II,III) oxide; magnetite; maghemite; TiO₂–Fe₃O₄; oxidation; photocatalysis



Citation: Krakowiak, R.; Frankowski, R.; Mylkie, K.; Mlynarczyk, D.T.; Ziegler-Borowska, M.; Zgoła-Grześkowiak, A.; Goslinski, T. TiO₂–Fe₃O₄ Composite Systems—Preparation, Physicochemical Characterization, and an Attempt to Explain the Limitations That Arise in Catalytic Applications. *Appl. Sci.* **2022**, *12*, 8826. <https://doi.org/10.3390/app12178826>

Academic Editor: Alberto Villa

Received: 11 August 2022

Accepted: 30 August 2022

Published: 2 September 2022

Publisher's Note: MDPI stays neutral with regard to jurisdictional claims in published maps and institutional affiliations.



Copyright: © 2022 by the authors. Licensee MDPI, Basel, Switzerland. This article is an open access article distributed under the terms and conditions of the Creative Commons Attribution (CC BY) license (<https://creativecommons.org/licenses/by/4.0/>).

1. Introduction

Titanium(IV) oxide (TiO₂) is a common metal oxide that finds many applications in different industries. It is used as an additive to paints, pharmaceuticals, and even food, mainly due to it being a material that is cheap, non-toxic, and broadly available [1,2]. On top of that, TiO₂ is one of the most commonly studied photocatalysts in photochemistry. This is a point of significant importance as the development of industry, and household use has introduced a new variety of chemical compounds into the environment. Ranging from chemical synthesis intermediates, by-products, active pharmaceutical ingredients, cosmetics, as well as insecticides and herbicides, these chemicals accumulate in soil and

water [3]. Although many of them are daily-use products and are safe for humans, such as pharmaceutical and personal care products, the effects of prolonged exposure to low concentrations of PPCPs are, for the most part, poorly documented and/or understood. Important to note that while PPCPs are safe for humans, exposure to low doses of these substances can be lethal for animals and lead to bio-accumulation in plants [4]. These substances, which are potential threats to the environment, were dubbed emerging contaminants and are now one of the most important topics in environmental chemistry [5]. In order to reduce the environmental threat, ways of remediating emerging contaminants are being sought. Photocatalysis is being investigated as one of such potential methods.

Bare TiO_2 can be used as an efficient UV-light photocatalyst, and its efficiency has been proven in a number of studies, even in the photodegradation of chemically stable emerging contaminants [3,6–8]. However, its broader uses in photocatalysis are limited by TiO_2 's physicochemical properties, mainly its relatively high band gap of anatase at 3.2 eV. A number of approaches can be chosen to modify the behavior of the material, such as surface modification, doping, and preparation of composite systems. The modifications allow for achieving new properties such as visible light activity or enhanced filtration potential through compositing with magnetic materials or by coating solid surfaces with functionalized TiO_2 composites.

One such modification is the preparation of TiO_2 - Fe_3O_4 composite systems. Iron(II,III) oxide is a ferrimagnetic metal oxide that naturally occurs in minerals such as magnetite. Similar to TiO_2 , Fe_3O_4 is commonly used as a pigment and also finds applications in medicine as part of contrast agents in magnetic resonance imaging [9]. Its magnetic nature is often the reason it is used for the functionalization of other materials. Therefore, TiO_2 - Fe_3O_4 composite systems have been researched in several studies in terms of photocatalytic efficiency, often revealing promising properties in the photodegradation reactions of organic dyes [10,11]. Not only that, one of the problems hindering TiO_2 research is the treatment of post-degradation slurry. In water solutions, TiO_2 forms milky suspensions, which are problematic to separate and, if not properly treated, pose a risk of environmental exposure. While generally safe for humans, it has been proven that exposure to TiO_2 might have adverse effects on aquatic life [12]. The magnetic properties of Fe_3O_4 allow for magnetic filtration of the photocatalyst after the photocatalytic process, thus reducing the above-mentioned threat.

Such composite materials can be prepared through a mechanochemical method—this method is particularly popular in the production of carbon nanotubes and nanofibers [13]. The method has been implemented in industrial processes due to its simplicity. Basic mechanochemical methods are two-step processes. First, two or more materials are milled together under specific conditions such as milling speed, milling duration, and temperature. Second, the ground-together materials are annealed in an oven in a gaseous atmosphere which can be either air or neutral gas, such as nitrogen or argon [14].

In this study, we present the preparation of a TiO_2 - Fe_3O_4 composite system and assess its potential use as a photocatalyst in the degradation of emerging contaminants, i.e., ibuprofen. We discuss difficulties associated with the use of Fe_3O_4 as a component of such composites, as well as processes occurring during the photocatalytic reaction in the context of the available literature data for similar materials.

2. Materials and Methods

Radleys Heat-On heating system (Saffron Walden, UK) was used for stirring reaction mixtures. Solvents and reagents were obtained from commercial suppliers (Merck, Darmstadt, Germany; Fluorochem, Hadfield, United Kingdom; Chempur, Piekary Śląskie, Poland; Avantor Performance Materials Poland S.A., Gliwice, Poland) and used without further purification. Anatase TiO_2 nanoparticles of 40 nm diameter were purchased from US Research Nanomaterials Inc., Houston, TX, USA. Mass spectrometry-grade methanol and ammonium acetate were purchased from Merck (Darmstadt, Germany). Mass spectrometry-grade water was prepared by reverse osmosis in a Demiwa system from Watek (Ledec nad Saza-

you, Czech Republic); the water underwent double distillation in a quartz apparatus. TiO₂-Fe₃O₄ composites were synthesized according to the procedures described below.

2.1. Preparation of TiO₂-Fe₃O₄

Fe₃O₄ was synthesized according to the following method: iron(II) chloride tetrahydrate (FeCl₂ × 4H₂O, 1 g, 5 mmol), and iron(III)chloride hexahydrate (FeCl₃ × 6H₂O, 2.7 g, 10 mmol) were added to a round-bottom flask containing distilled water (12.5 mL) and hydrochloric acid (HCl, 0.187 g, 5.15 mmol). Next, sodium hydroxide (NaOH, 1.5 M) water solution was added dropwise into the flask until a black product was formed. The black product (Fe₃O₄) was recovered from the suspension by applying a magnet, washed with deionized water, and dried under a vacuum at 30 °C for 24 h.

TiO₂-Fe₃O₄ was prepared by mechanochemical method by grinding Fe₃O₄ and TiO₂ (anatase, 40 nm) in a 1:1 weight ratio to receive a fine homogenous grey powder. Next, the grey powder was put into a muffle oven for an annealing process at 200 °C for 4 h in an air atmosphere.

2.2. Characterization of TiO₂-Fe₃O₄

2.2.1. Morphological Studies with Electron Microscopy

Scanning electron microscopy (SEM) images were captured with FEI Quanta 3D FEG (FEI, Hillsboro, OR, USA) with an acceleration voltage of 20 kV.

2.2.2. X-ray Powder Diffractometry

X-ray powder diffractometry (XRPD) measurements were performed with X'Pert Pro-diffractometer by Malvern Panalytical (Malvern, United Kingdom) with X'Celerator Scientific detector, Cu-Kα X-ray radiation, and data for the 2θ range from 5° to 120° with a step of 0.008°.

2.2.3. Thermogravimetric Analysis

Thermogravimetric analysis (TGA) was performed with STA 449 F5 Jupiter (Netzsch, Selb, Germany). The measurements were conducted at a 10 °C × min⁻¹ heating rate in the range from 25 °C to 635 °C in the atmosphere of air.

2.2.4. Nanoparticle Tracking Analysis

Nanoparticle tracking analysis (NTA) was performed with Malvern Panalytical (Malvern, UK) NanoSight LM10 instrument (sCMOS camera, 405 nm laser) using NTA (Nanoparticle Tracking Analysis) 3.2 Dev Build 3.2.16 software. The samples were diluted with distilled water to the operating range of the device. All samples were sonicated and vortexed before measurements to assure uniform distribution of the particles within the suspension. Temperature control was enabled and maintained at 25.0 ± 0.1 °C. The syringe pump infusion rate was set to 200 μL × min⁻¹. For each sample 5 × 60 s videos were recorded.

2.3. Measurements of Photocatalytic Activity

Ibuprofen (IBU) water solution was prepared at a concentration of 10 mg/L. For all tests, 1 g/L of the composite photocatalyst was chosen as the concentration for photoactivity tests. IBU solution (30 mL) and photocatalyst (30 mg) were added to three separate vials each. The solutions were sonicated before placement in the reactor. First, the solution was stirred in the dark for 30 min to set adsorption-desorption equilibrium and to test the dark activity. After that, the LED lamps were turned on, and the mixture was irradiated for 2 h while under constant stirring. During the tests, 1 mL samples were taken at times of -0.5 h, 0 h, 0.5 h, 1 h, and 2 h. The temperature of the system was controlled and did not exceed 25 °C.

Photocatalytic activity tests were performed with Photocube by ThalesNano (Budapest, Hungary). Irradiations were conducted using four diode panels emitting light with the wavelength of 365 nm (UV) or 523 nm (G), depending on the test. The lamps were operating

at full power, achieving 128 W per color as described by the producer. The samples were stored in a refrigerator at 8 °C before and after measurements.

2.4. LC-MS/MS: Sample Preparation and Analysis

Samples from photocatalytic tests were centrifuged, diluted 20 times with 50% methanol, and filtered through a 0.2 µm PTFE syringe filter. LC-MS/MS analysis was conducted on an UltiMate 3000 liquid chromatograph from Dionex (Sunnyvale, CA, USA) coupled with an API 4000 QTRAP tandem mass spectrometer from Applied Biosystems/MDS Sciex (Waltham, MA, USA). A Synergi Fusion RP column (50 mm × 2.0 mm I.D.; 2.5 µm) from Phenomenex (Torrance, CA, USA) was used for chromatographic separation, onto which 5 µL of the sample was injected at a mobile phase flow rate of 0.3 mL/min. The chromatograph worked in a mobile phase gradient consisting of a 5 mM solution of ammonium acetate in water (A) and methanol (B). The initial phase composition was set at 70% B, then it was ramped up to 100% B over 2.5 min and held for 0.5 min. Analysis was performed under a constant temperature of 35 °C. The eluate from the column was directed to the mass spectrometer through an electrospray ion source operated in the negative ion mode. The source and spectrometer parameters were set as follows: curtain gas pressure 10 psi, nebulizing gas pressure 40 psi, auxiliary gas pressure 40 psi, temperature 400 °C, electrospray voltage −3500 V, declustering potential −35 V, and collision gas was set to medium. The mass spectrometer was operated in the multiple reaction monitoring (MRM) mode. The ion transition from 205 to 161 m/z was selected with a collision energy of −10 eV.

2.5. Acute Toxicity Assay

TiO₂, Fe₃O₄, and TiO₂-Fe₃O₄ samples were tested with Microtox acute toxicity test–81.9% Screening Test, which was performed using Microtox M500 equipment according to the protocols distributed by the producer (ModernWater plc, London, United Kingdom) [15,16]. Cell viability was calculated according to bioluminescence emitted by the *Aliivibrio fischeri* bacteria as measured with Microtox M500 with Modern Water MicrotoxOmni 4.2 software.

3. Results and Discussion

3.1. Preparation and Characterization of the Material

3.1.1. Preparation of TiO₂-Fe₃O₄ Composite

A composite material based on titanium(IV) oxide and iron(II,III) oxide was prepared by mechanochemical method. After the annealing process, slight browning of the material was noted and associated with oxidation of magnetite Fe₃O₄ into maghemite γ-Fe₂O₃.

3.1.2. Morphological Studies

SEM micrographs (Figure 1) were used to study the surface morphology of the prepared composite material. SEM images of bare TiO₂ show tightly packed clusters of aggregates of the core 40 nm particles. The micrographs for TiO₂ show particles that appear pseudospherical in shape, which is one of the characteristic forms for unmodified anatase [17]. TiO₂-Fe₃O₄ particles reveal similar aggregation behavior as bare TiO₂. In the case of TiO₂-Fe₃O₄, it appears that TiO₂ particles were grafted onto much bigger, micrometric particles of Fe₃O₄, forming a coating over Fe₃O₄'s surface similar to a core-shell structure. The synthesized Fe₃O₄ was expected to have a much more spherical shape. However, based on the micrographs, it can be said that the magnetite took the shape of irregular, micrometric grain aggregates.

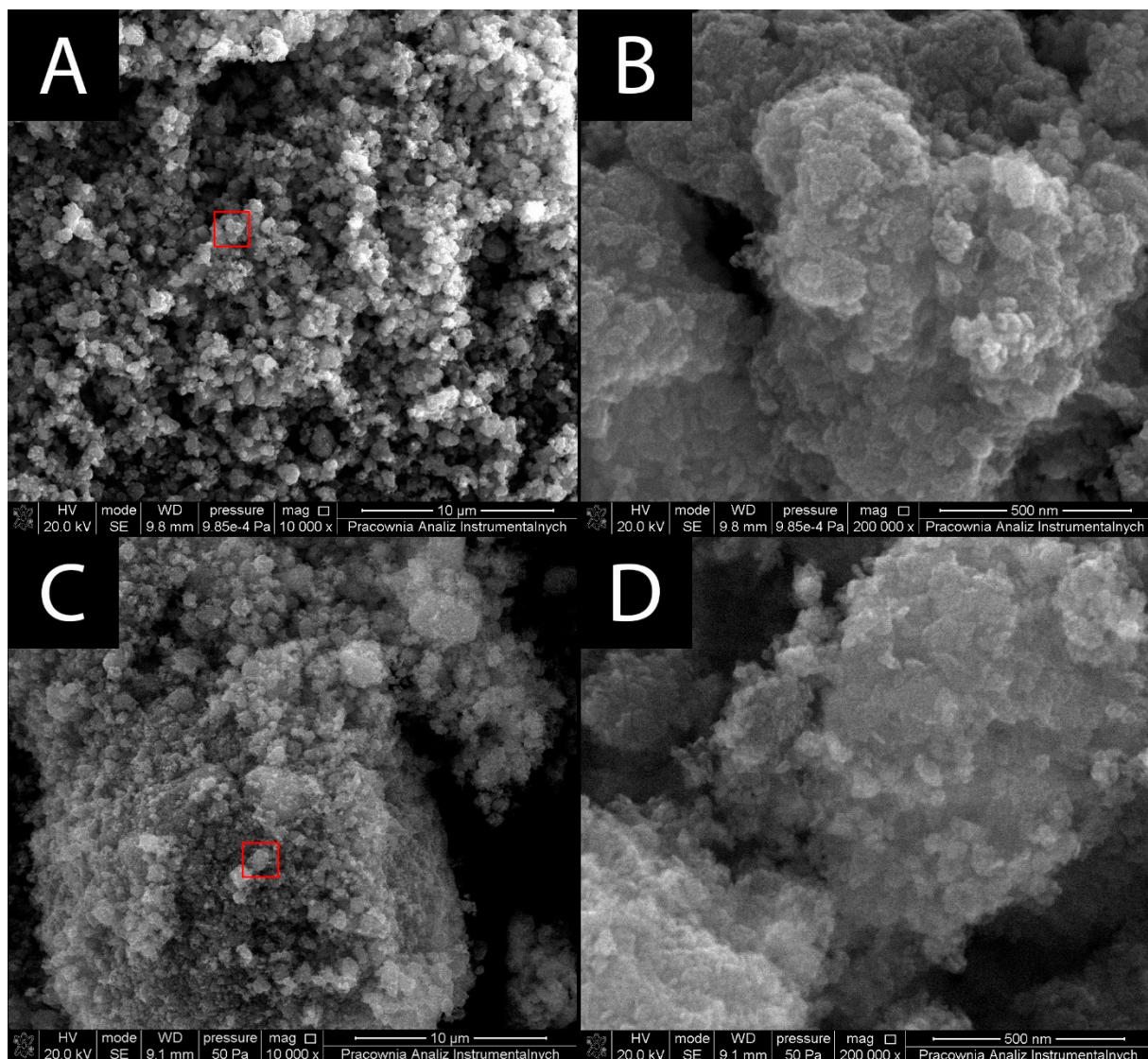


Figure 1. SEM micrographs of bare TiO_2 and $\text{TiO}_2\text{-Fe}_3\text{O}_4$ composite material. (A) Microscale image of bare TiO_2 (magnification $10,000\times$), (B) nanoscale image of TiO_2 (magnification $200,000\times$), (C) microscale image of $\text{TiO}_2\text{-Fe}_3\text{O}_4$ (magnification $10,000\times$), and (D) nanoscale image of $\text{TiO}_2\text{-Fe}_3\text{O}_4$ (magnification $200,000\times$). Red boxes in A and C show the enlarged areas in B and D, respectively.

3.1.3. Hydrodynamic Size

The hydrodynamic size of the materials was evaluated with the NanoSight LM10 apparatus, and the results are presented in Figure 2 and Table 1. The assay portrays the aggregation behavior of the composite material within water suspension. While SEM provides insight into the size and morphology of the material in dry form, the results might differ in a water suspension due to factors such as aggregation. In addition, before NTA, solid materials have to undergo treatment such as sonicating and vortexing to allow uniform distribution of the particles within the suspension for accurate measurements. Based on the results, it can be concluded that all materials show a high tendency for aggregation, especially evident in the case of $\text{TiO}_2\text{-Fe}_3\text{O}_4$, which presents an average particle size of around 369.5 nm. This fact could explain the high standard deviation values of 232.9 nm noted for $\text{TiO}_2\text{-Fe}_3\text{O}_4$ particles. Polydispersity indices were calculated for both TiO_2 and $\text{TiO}_2\text{-Fe}_3\text{O}_4$ materials. In all cases, PDI exceeds the value of 0.2, which is treated as the threshold for labeling material as monodisperse; as such, all materials were considered polydisperse.

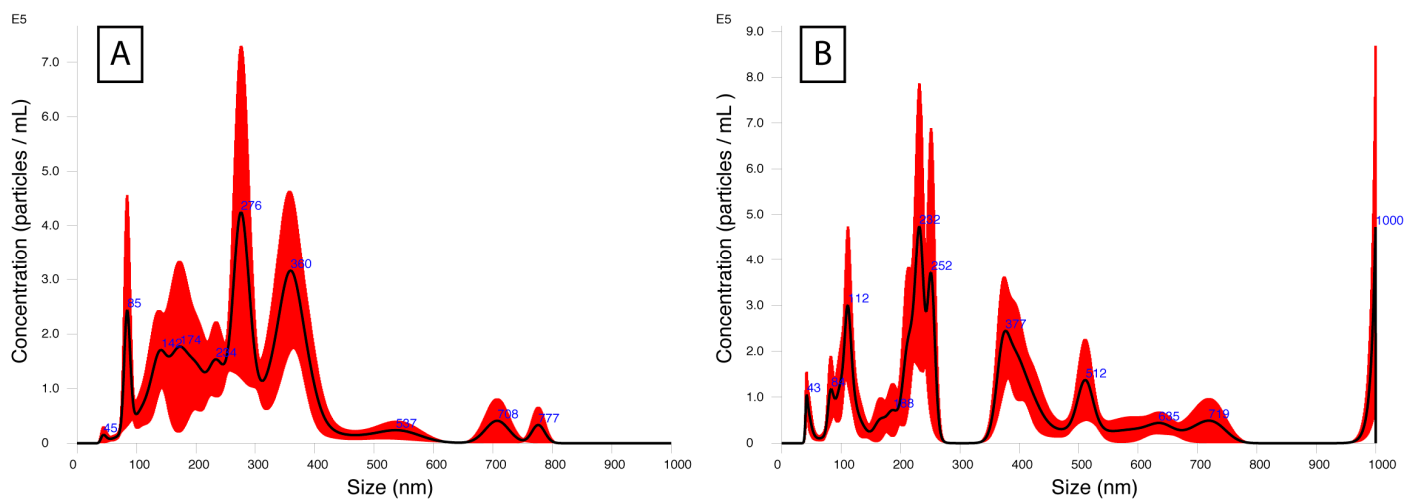


Figure 2. Hydrodynamic size measurements with NTA. The graph shows particle size distribution in the range of 0–1000 nm for (A) bare TiO₂ and (B) TiO₂–Fe₃O₄.

Table 1. Hydrodynamic size analysis of the composite materials with NTA.

Material	Particle Size (Mean ± SD)	PDI ^a
TiO ₂	190.9 ± 103.4 nm	0.293
TiO ₂ –Fe ₃ O ₄	369.5 ± 232.9 nm	0.397

SD—standard deviation; PDI—polydispersity index; ^a calculated according to the formula (SD/Mean)².

3.1.4. XRPD

The crystallinity of the materials was investigated with XRPD (Figure 3). Results obtained for bare TiO₂ are in agreement with JCPDS card no. 21-1272 for anatase and show reflections at 25.47, 37.97, 48.21, 54.09, 55.24, 62.95, 68.89, 70.47, 75.31° [18]. Additional reflections coming from admixture of Fe₃O₄ can be noted in the composite material at 35.76°, 57.19°, 62.95°. The reflection at 30.42° can be assigned both to Fe₃O₄ and Fe₂O₃, which is created as a result of Fe₃O₄ oxidation during exposure to air [19]. In addition, the composite revealed further changes in the XRPD spectrum. It especially concerns the shifting of the peaks at 38° and 48° towards lower values, which is the evidence for the material's crystallinity being impacted as a result of functionalization with Fe₃O₄.

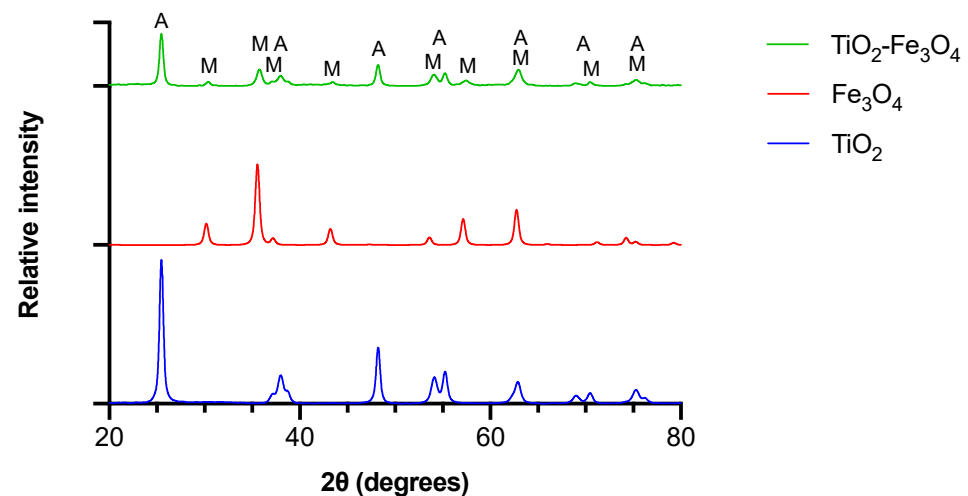


Figure 3. X-ray powder diffraction patterns of bare TiO₂, Fe₃O₄ and TiO₂–Fe₃O₄ composite materials. A—reflection corresponding to anatase TiO₂, M—reflection corresponding to magnetite Fe₃O₄.

3.1.5. Thermogravimetric Analysis

All materials were evaluated with thermogravimetric analysis (Figure 4). The results are summarized in Table 2.

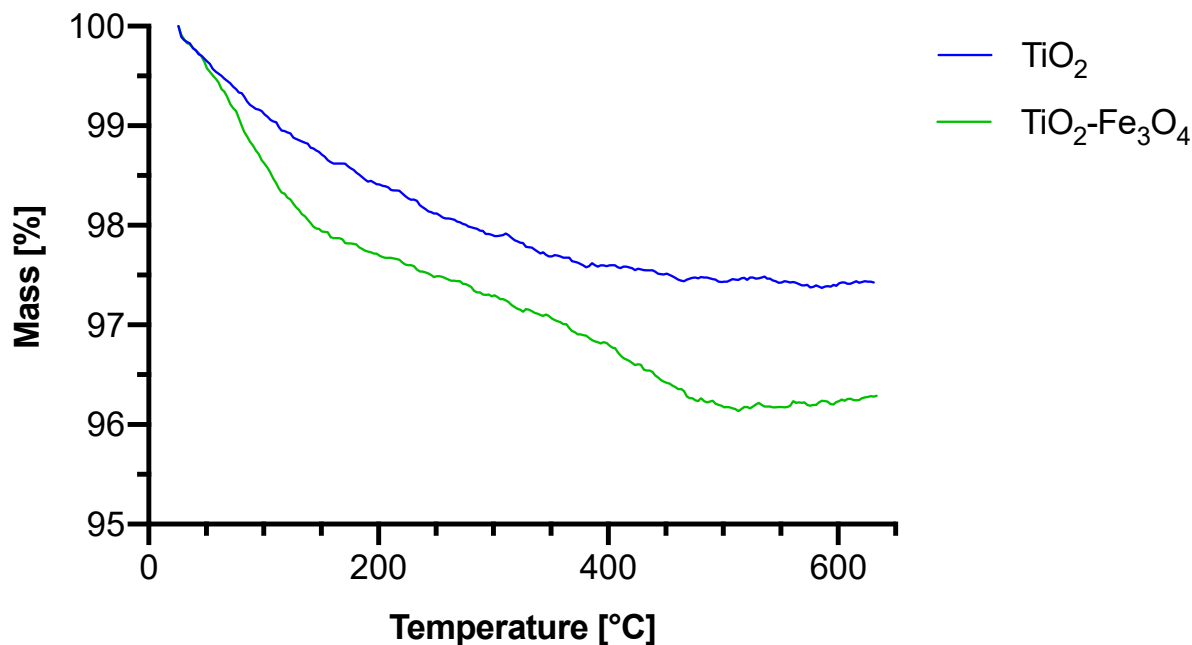


Figure 4. Thermogravimetric analysis graphs of bare TiO_2 and $\text{TiO}_2\text{-Fe}_3\text{O}_4$ composite materials.

Table 2. Thermogravimetric analysis of bare TiO_2 and $\text{TiO}_2\text{-Fe}_3\text{O}_4$ composite materials.

Material	First Stage			Second Stage			Residue (%)
	T_p (°C)	T_k (°C)	Δm (%)	T_p (°C)	T_k (°C)	Δm (%)	
TiO_2	26	384	2.51				97.49
$\text{TiO}_2\text{-Fe}_3\text{O}_4$	26	187	2.24	188	635	1.45	96.31

For bare TiO_2 , one stage in the range of 26–384 °C with 2.51% mass loss was noted, and the mass loss can be associated with the evaporation of surface water. For the composite material, the thermal decomposition of $\text{TiO}_2\text{-Fe}_3\text{O}_4$ reveals two stages. The first stage begins at 26 °C and ends at 187 °C with a mass loss of 2.24%, whereas the second stage appears in the range of 188–635 °C with a resulting mass loss of 1.45%. The first stage can be associated with the evaporation of water residue from the surface of TiO_2 . The mass changes in the second stage result from the condensation of surface hydroxyl groups within TiO_2 [20], similarly to bare TiO_2 , but in the composite material, this process is split between the two stages. Based on literature data, Fe_3O_4 is known to not undergo any decomposition and only lose moisture [21]. While exposed to air, any mass changes coming from the oxidation process of Fe_3O_4 into Fe_2O_3 overlap with the changes associated with the evaporation of surface water.

3.2. Photocatalytic Activity of $\text{TiO}_2\text{-Fe}_3\text{O}_4$ Composite systems

One of the main reasons for the functionalization of TiO_2 either by surface modification, doping, or by preparing composite systems is to alleviate its flaws, including very weak photoactivity in visible light or troublesome filtration after the remediation processes. By preparing $\text{TiO}_2\text{-Fe}_3\text{O}_4$ composites, these imperfections can be at least partially abolished. $\text{TiO}_2\text{-Fe}_3\text{O}_4$ composites possess a paramagnetic property that allows for the photocatalyst's filtration with a magnetic field after the photocatalytic reaction. Additionally, due to the

band gap of Fe_3O_4 , $\text{TiO}_2\text{-Fe}_3\text{O}_4$ composites should reveal photoactivity after irradiation with visible light [22,23].

Photocatalytic degradation tests of ibuprofen with bare TiO_2 and $\text{TiO}_2\text{-Fe}_3\text{O}_4$ composite material under irradiation with UV light (365 nm) and green light (523 nm) are presented in Figure 5. Photodegradation tests with UV light (Figure 5A) revealed impaired photoactivity of the composite material in comparison to bare TiO_2 . The negative effect was observed both under UV and green light irradiations. After 2 h of irradiation with the UV light in the presence of bare TiO_2 , a 44% reduction of initial ibuprofen concentration was noted, whereas in the presence of $\text{TiO}_2\text{-Fe}_3\text{O}_4$, only a 19% reduction appeared. At the beginning of the experiment, both materials show comparable degradation rates. However, after 1 h of irradiation with $\text{TiO}_2\text{-Fe}_3\text{O}_4$, a plateau is reached.

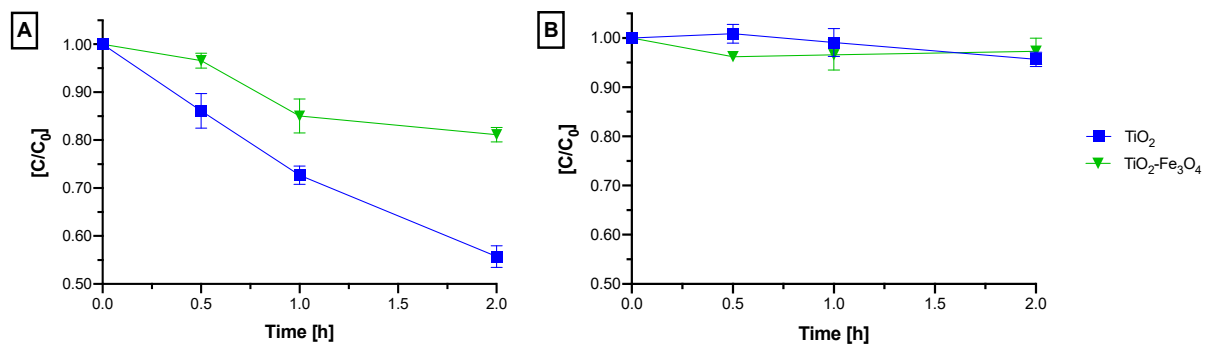


Figure 5. Photocatalytic degradation tests of ibuprofen with bare TiO_2 and $\text{TiO}_2\text{-Fe}_3\text{O}_4$ composite material under irradiation with (A) UV light (365 nm) and (B) green light (523 nm).

After 2 h of irradiation with green light in the presence of bare TiO_2 only a mean 4% ibuprofen degradation rate was achieved (Figure 5B). The obtained result could be considered statistically insignificant and treated as a lack of activity. Interestingly, the composite showed only comparable photoactivity in green light as bare TiO_2 . The result is contradictory to the expected effect as the Fe_3O_4 band gap should allow the absorption of wavelengths from the green light region [22] and subsequent sensitization of TiO_2 . Initially, $\text{TiO}_2\text{-Fe}_3\text{O}_4$ showed much better degradation rates of ibuprofen than bare TiO_2 . However, after 1 h time, the ibuprofen concentration slightly increased, indicating that the photocatalytic reaction stopped and that ibuprofen desorbed from the photocatalyst's surface back to the reaction suspension. After 2 h of irradiation, only a 3% IBU degradation rate was noted with $\text{TiO}_2\text{-Fe}_3\text{O}_4$. The disappearance of $\text{TiO}_2\text{-Fe}_3\text{O}_4$ photoactivity in both irradiation tests was accompanied by the browning of the $\text{TiO}_2\text{-Fe}_3\text{O}_4$ material during irradiation which is associated with the oxidation of Fe_3O_4 within the photosensitizer to maghemite ($\gamma\text{-Fe}_2\text{O}_3$).

The process can be explained as follows: after irradiation of TiO_2 with light (1), photons that have higher energy than the TiO_2 bandgap are absorbed, and the energy is consumed for the transition of TiO_2 unpaired electrons from the valence band to the conduction band. The conduction band electrons interact with surface oxygen leading to the creation of superoxide radicals (2), which then react with Fe_3O_4 within the composite system leading to the transformation of magnetite to maghemite (3) [3,24].

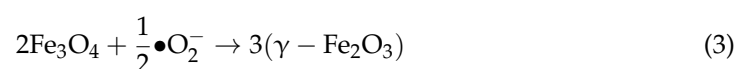


Figure 6 shows the proposed mechanism of the above-mentioned process. Due to the transformation of Fe_3O_4 to $\gamma\text{-Fe}_2\text{O}_3$ within the composite material during the irra-

diation process, the ROS produced in the process are consumed during the oxidative transformation of magnetite to maghemite instead of being used in the photodegradation of model pollutant, i.e., ibuprofen. This leads to lowered photodegradation rates. Table 3 shows the comparison to findings reported in similar studies where $\text{TiO}_2\text{-Fe}_3\text{O}_4$ was used in photocatalysis.

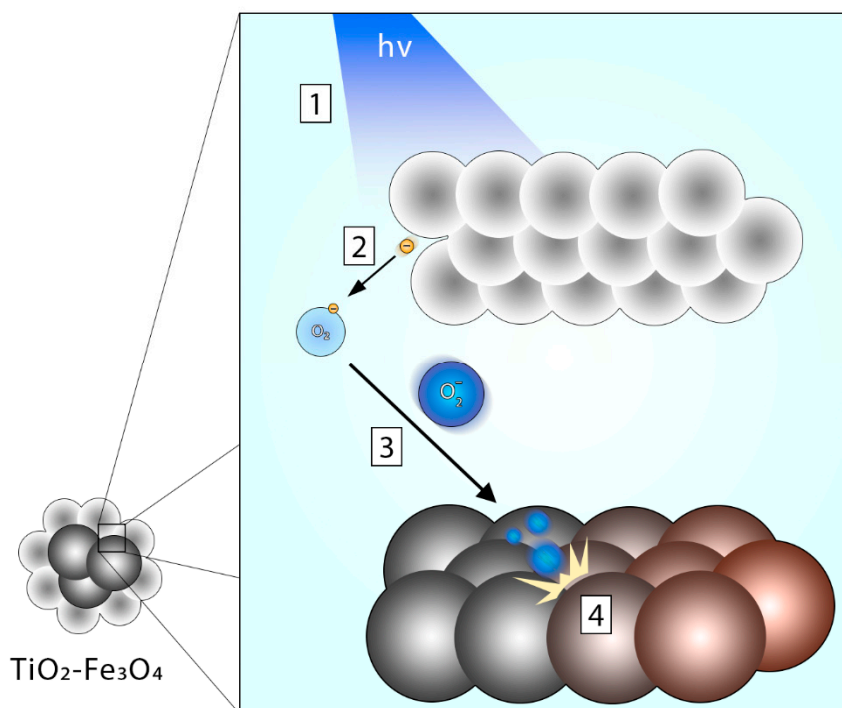


Figure 6. Photooxidative transformation of Fe_3O_4 into $\gamma\text{-Fe}_2\text{O}_3$ in a $\text{TiO}_2\text{-Fe}_3\text{O}_4$ composite system. The proposed mechanism of the process is as follows: (1) conduction band electrons and electron holes are formed as a consequence of irradiation of the TiO_2 layer; (2) the electrons interact with oxygen present in the reaction environment producing superoxide radicals; (3) superoxide radicals interact with Fe_3O_4 atoms leading to (4) its oxidation into $\gamma\text{-Fe}_2\text{O}_3$.

Table 3. $\text{TiO}_2\text{-Fe}_3\text{O}_4$ usage in photocatalysis.

Material ^a	Method of Preparation	Photocatalytic Substrate	Irradiation Wavelength	Reaction Time	TiO_2 Photoefficiency ^b	$\text{TiO}_2\text{-Fe}_3\text{O}_4$ Photoefficiency ^b	Reference
$\text{TiO}_2\text{-Fe}_3\text{O}_4$	Mechano-thermal	Ibuprofen	365, 523 nm	2 h	44%, <5%	19%, <5%	This study
$\text{Fe}_x\text{O}_y/\text{TiO}_2$	Impregnation	Chloroform	365 nm	10 h	~60%	~30%	[25]
$\text{Fe}_3\text{O}_4/\text{TiO}_2$	Not indicated	BPA	365 nm	2 h	56%	50%	[26]
$\text{Fe}_3\text{O}_4@\text{TiO}_2$	Vapor-thermal	Rhodamine B	UV	1 h	~85%	~35%	[27]
FeTiNC	Pulsed laser deposition	Cr(VI) ions	UV, Vis > 380 nm	2 h	24%, 3% [28]	69%, 19%	[29]
$\text{TiO}_2/\text{Fe}_3\text{O}_4$	Ultrasonic	Orange G	Vis	2 h	~20%	~60%	[30]
$\text{TiO}_2/\text{Fe}_3\text{O}_4$	Ultrasonic	Paracetamol	254 nm	5 h	~95%	~89%	[31]

^a as referred to in the referenced source material, ^b photoefficiencies are listed in order of irradiation wavelengths as reductions of initial concentration of the substrate, BPA–bisphenol A.

A similar effect could be observed in a different study where the effect of $\text{Fe}_x\text{O}_y/\text{TiO}_2$ on the photodegradation of CHCl_3 was investigated [25]. Although $\text{Fe}_x\text{O}_y/\text{TiO}_2$ synthesized by hydrothermal method showed similar degradation rates to bare TiO_2 , $\text{Fe}_x\text{O}_y/\text{TiO}_2$ prepared by an impregnation method revealed worse rates than bare TiO_2 . Another study reports that the addition of Fe_3O_4 to TiO_2 reduced the system's efficiency in removing bisphenol A (BPA) under UV-A irradiation in a photocatalytic, non-Fenton system. Based

on that observation, the researchers concluded that magnetite does not reduce the energy gap of titania or improve the recombination of e^- - h^+ holes, as well as reduces the ability of the system to form hydroxyl radicals [26]. A different study reports similar findings in the degradation of rhodamine B [27]. However, in another study, composite films based on TiO_2 and Fe_2O_3 or Fe_3O_4 and co-doped with N and C atoms revealed better photocatalytic reduction rates of dichromate ions by the materials where Fe_3O_4 was applied [29]. In a study by Alvarez et al. [31], TiO_2 - Fe_3O_4 was used for photodegradation of acetaminophen under UV light. Although the achieved degradation rates were high, the TiO_2 - Fe_3O_4 performed worse than bare TiO_2 . Only after co-compositing with SiO_2 , the rates approached the ones achieved by bare TiO_2 . This only reinforces the notion that for efficient use of Fe_3O_4 in composite materials, the use of a co-dopant that would stabilize its oxidation-prone ions is required. To sum up, in photochemical applications, especially photodegradation of organic compounds, the presence of Fe(II) ions instead of Fe(III) seems to be more favorable. It is due to the fact that Fe(II) ions are more prone to oxidation processes.

3.3. Acute Toxicity

The acute toxicity of the material was investigated through a Microtox protocol, and the results are presented in Figure 7. Materials that showed inhibition rates under 20% were treated as non-toxic [32]. Bare TiO_2 reveals negligible toxicity to *A. fischerii*, even at 1% concentration, 10 times higher than the concentration of the photocatalysts used in the photocatalytic tests. Interestingly, a slight hormetic effect can also be noted for TiO_2 , which then decreases with a prolonged time of exposure. It is interesting that the toxic effect of Fe_3O_4 was reduced after grafting it on TiO_2 . These results are in line with those previously reported in the literature, including the ability of TiO_2 to reduce the acute toxicity of other metal particles [16].

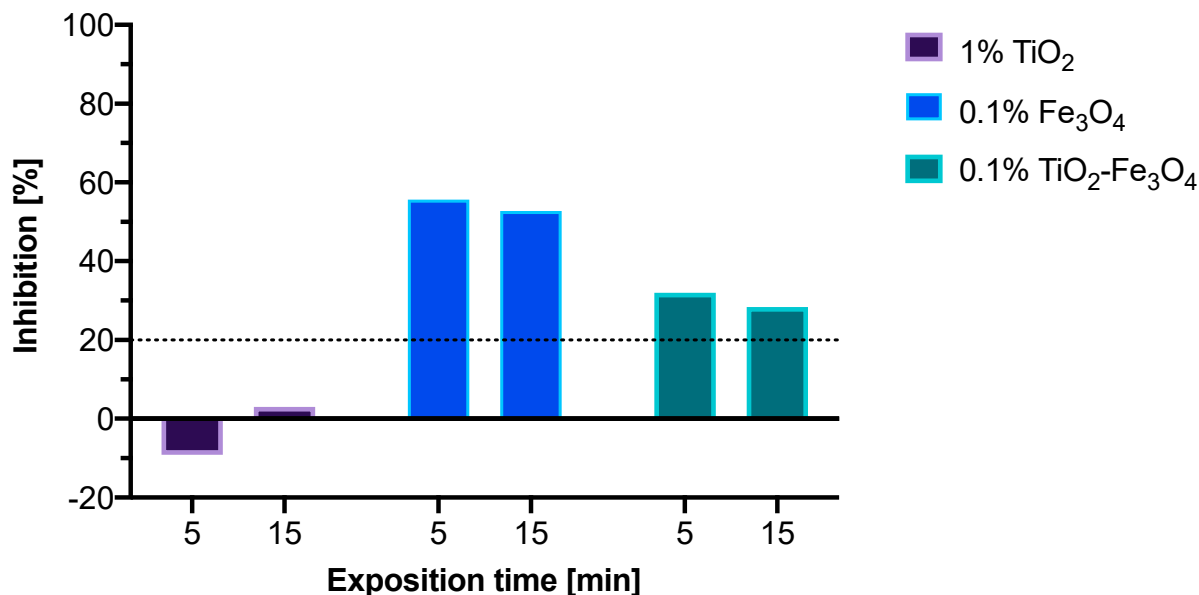


Figure 7. Acute toxicity assay of TiO_2 , Fe_3O_4 , and TiO_2 - Fe_3O_4 composite material.

4. Conclusions

TiO_2 - Fe_3O_4 composite system was prepared through a mechanochemical method and fully characterized. The composite material was annealed in a muffle oven at 200 °C for 4 h. Photoactivity of the composite material was compared to bare TiO_2 in photocatalytic degradation tests of ibuprofen. The photocatalytic tests revealed inferior photoactivity of the composite material in UV light (19% photodegradation rate) as compared to bare TiO_2 (44% degradation rate) and no statistically significant photoactivity for either material in visible light tests. As a consequence of irradiation, browning of the suspensions was noted,

which grew with longer exposure times. The effect was explained by further oxidation of magnetite Fe_3O_4 into maghemite $\gamma\text{-Fe}_2\text{O}_3$ caused by reactive oxygen species produced as a result of irradiation of the material with UV or visible light. As ROS play a key role in the photodegradation of organic substances in photocatalysis, the photodegradation rates of ibuprofen were negatively impacted after the ROS were consumed in a different process. Although the composite retained its magnetic properties, it could not be used as an efficient photocatalyst. To fully take advantage of this material, further modification should be considered that would stabilize the composite and prevent oxidation of Fe_3O_4 into $\gamma\text{-Fe}_2\text{O}_3$. Alternatively, the preparation of $\text{TiO}_2\text{-}\gamma\text{-Fe}_2\text{O}_3$ could be considered, as maghemite seems a much more stable substitute for photocatalytic applications, including photodegradation of organic compounds. Microtox acute toxicity assay allowed to confirm that TiO_2 can reduce ecotoxicity of other metal oxides, such as Fe_3O_4 . We noted for $\text{TiO}_2\text{-Fe}_3\text{O}_4$ that inhibition rates of the *Aliivibrio fischeri* bacteria cell viability fell from 56% to 32% according to bioluminescence emitted, which falls in line with available literature data.

Author Contributions: Conceptualization: R.K., T.G., A.Z.-G. and M.Z.-B.; Methodology: R.K.; Software: R.K.; Validation: R.K. and A.Z.-G.; Formal analysis: R.K. and A.Z.-G.; Investigation: R.K., R.F., K.M. and D.T.M.; Resources: R.K., T.G., A.Z.-G. and M.Z.-B.; Data curation: R.K., R.F., K.M., D.T.M., T.G., A.Z.-G. and M.Z.-B.; Writing—original draft preparation: R.K.; Writing—review and editing: R.K., D.T.M., T.G., A.Z.-G. and M.Z.-B.; Visualization: R.K.; Supervision: R.K. and T.G.; Project administration: R.K.; Funding acquisition: R.K. All authors have read and agreed to the published version of the manuscript.

Funding: The research was financed by a small research grant from the Poznan University of Medical Sciences statutory funding for young researchers—doctoral students (Grant no. SDUM-GB31/03/21). Rafał Krakowiak is a doctoral student of the NanoBioTech Interdisciplinary Doctoral Program as a part of the Knowledge Education and Development 2014–2020 operational program financed by the European Social Fund (Grant no. POWR.03.02.00-00-I011/16).

Institutional Review Board Statement: Not applicable.

Informed Consent Statement: Not applicable.

Data Availability Statement: Data will be made available on request.

Conflicts of Interest: The authors declare no conflict of interest. The funders had no role in the design of the study; in the collection, analyses, or interpretation of data; in the writing of the manuscript; or in the decision to publish the results.

References

1. Jovanović, B. Critical Review of Public Health Regulations of Titanium Dioxide, a Human Food Additive. *Integr. Environ. Assess. Manag.* **2015**, *11*, 10–20. [[CrossRef](#)] [[PubMed](#)]
2. Musiał, J.; Krakowiak, R.; Młynarczyk, D.T.; Goslinski, T.; Stanisław, B.J. Titanium Dioxide Nanoparticles in Food and Personal Care Products—What Do We Know about Their Safety? *Nanomaterials* **2020**, *10*, 1110. [[CrossRef](#)] [[PubMed](#)]
3. Krakowiak, R.; Musiał, J.; Bakun, P.; Sychała, M.; Czarzynska-Goslinska, B.; Młynarczyk, D.T.; Koczorowski, T.; Sobotta, L.; Stanisław, B.; Goslinski, T. Titanium Dioxide-Based Photocatalysts for Degradation of Emerging Contaminants Including Pharmaceutical Pollutants. *Appl. Sci.* **2021**, *11*, 8674. [[CrossRef](#)]
4. Wilkinson, J.L.; Hooda, P.S.; Barker, J.; Barton, S.; Swinden, J. Ecotoxic Pharmaceuticals, Personal Care Products, and Other Emerging Contaminants: A Review of Environmental, Receptor-Mediated, Developmental, and Epigenetic Toxicity with Discussion of Proposed Toxicity to Humans. *Crit. Rev. Environ. Sci. Technol.* **2016**, *46*, 336–381. [[CrossRef](#)]
5. Sarma, H.; Lee, W.-Y.; Domínguez, D.C. *Emerging Contaminants in the Environment: Challenges and Sustainable Practices*; Elsevier: Amsterdam, The Netherlands, 2022; p. 687.
6. Davit, P.; Martra, G.; Coluccia, S. Photocatalytic Degradation of Organic Compounds on TiO_2 Powders FT-IR Investigation of Surface Reactivity and Mechanistic Aspects. *J. Jpn. Pet. Inst.* **2004**, *47*, 359–376. [[CrossRef](#)]
7. Chen, C.; Lu, C.; Chung, Y.; Jan, J. UV Light Induced Photodegradation of Malachite Green on TiO_2 Nanoparticles. *J. Haz. Mat.* **2007**, *141*, 520–528. [[CrossRef](#)]
8. Liu, Y.; Gan, X.; Zhou, B.; Xiong, B.; Li, J.; Dong, C.; Bai, J.; Cai, W. Photoelectrocatalytic Degradation of Tetracycline by Highly Effective TiO_2 Nanopore Arrays Electrode. *J. Haz. Mat.* **2009**, *171*, 678–683. [[CrossRef](#)]
9. Ganapathe, L.S.; Mohamed, M.A.; Mohamad Yunus, R.; Berhanuddin, D.D. Magnetite (Fe_3O_4) Nanoparticles in Biomedical Application: From Synthesis to Surface Functionalisation. *Magnetochemistry* **2020**, *6*, 68. [[CrossRef](#)]

10. Zhang, H.; He, X.; Zhao, W.; Peng, Y.; Sun, D.; Li, H.; Wang, X. Preparation of Fe₃O₄/TiO₂ Magnetic Mesoporous Composites for Photocatalytic Degradation of Organic Pollutants. *Water Sci. Technol.* **2017**, *75*, 1523–1528. [[CrossRef](#)]
11. Vinosek, V.M.; Anand, S.; Janifer, M.A.; Pauline, S.; Dhanavel, S.; Praveena, P.; Stephen, A. Preparation and Performance of Fe₃O₄/TiO₂ Nanocomposite with Enhanced Photo-Fenton Activity for Photocatalysis by Facile Hydrothermal Method. *Appl. Phys. A* **2019**, *125*, 319. [[CrossRef](#)]
12. Bobori, D.; Dimitriadi, A.; Karasiali, S.; Tsoumaki-Tsouroufli, P.; Mastora, M.; Kastrinaki, G.; Feidantsis, K.; Printzi, A.; Koumoundouros, G.; Kaloyianni, M. Common Mechanisms Activated in the Tissues of Aquatic and Terrestrial Animal Models after TiO₂ Nanoparticles Exposure. *Environ. Int.* **2020**, *138*, 105611. [[CrossRef](#)]
13. Manafi, S.; Rahimpour, M.R.; Mobasherpour, I.; Soltanmoradi, A. The Synthesis of Peculiar Structure of Springlike Multiwall Carbon Nanofibers/Nanotubes via Mechanochemical Method. *J. Nanomater.* **2012**, *2012*, 803546. [[CrossRef](#)]
14. Soares, O.S.G.P.; Rocha, R.P.; Órfão, J.J.M.; Pereira, M.F.R.; Figueiredo, J.L. Mechanochemical Approach for N-, S-, P-, and B-Doping of Carbon Nanotubes: Methodology and Catalytic Performance in Wet Air Oxidation. *C* **2019**, *5*, 30. [[CrossRef](#)]
15. Thomas Johnson, B. Microtox® Acute Toxicity Test. In *Small-Scale Freshwater Toxicity Investigations: Volume 1-Toxicity Test Methods*; Blaise, C., Féraud, J.-F., Eds.; Springer: Dordrecht, The Netherlands, 2005; pp. 69–105. ISBN 978-1-4020-3119-9.
16. Recillas, S.; García, A.; González, E.; Casals, E.; Puentes, V.; Sánchez, A.; Font, X. Use of CeO₂, TiO₂ and Fe₃O₄ Nanoparticles for the Removal of Lead from Water: Toxicity of Nanoparticles and Derived Compounds. *Desalination* **2011**, *277*, 213–220. [[CrossRef](#)]
17. Dozzi, M.V.; Montalbano, M.; Marra, G.; Mino, L.; Selli, E. Effects of Anatase TiO₂ Morphology and Surface Fluorination on Environmentally Relevant Photocatalytic Reduction and Oxidation Reactions. *Mater. Today Chem.* **2021**, *22*, 100624. [[CrossRef](#)]
18. He, J.; Du, Y.; Bai, Y.; An, J.; Cai, X.; Chen, Y.; Wang, P.; Yang, X.; Feng, Q. Facile Formation of Anatase/Rutile TiO₂ Nanocomposites with Enhanced Photocatalytic Activity. *Molecules* **2019**, *24*, 2996. [[CrossRef](#)]
19. Lemine, O.M.; Madkhali, N.; Alshammari, M.; Algessair, S.; Gismelseed, A.; El Mir, L.; Hjiri, M.; Yousif, A.A.; El-Boubbou, K. Maghemite (γ-Fe₂O₃) and γ-Fe₂O₃-TiO₂ Nanoparticles for Magnetic Hyperthermia Applications: Synthesis, Characterization and Heating Efficiency. *Materials* **2021**, *14*, 5691. [[CrossRef](#)]
20. Li, X.W.; Song, R.G.; Jiang, Y.; Wang, C.; Jiang, D. Surface Modification of TiO₂ Nanoparticles and Its Effect on the Properties of Fluoropolymer/TiO₂ Nanocomposite Coatings. *Appl. Surf. Sci.* **2013**, *276*, 761–768. [[CrossRef](#)]
21. Stoia, M.; Istrate, R.; Păcurariu, C. Investigation of Magnetite Nanoparticles Stability in Air by Thermal Analysis and FTIR Spectroscopy. *J. Therm. Anal. Calorim.* **2016**, *125*, 1185–1198. [[CrossRef](#)]
22. Bagbi, Y.; Sarswat, A.; Mohan, D.; Pandey, A.; Solanki, P.R. Lead and Chromium Adsorption from Water Using L-Cysteine Functionalized Magnetite (Fe₃O₄) Nanoparticles. *Sci. Rep.* **2017**, *7*, 7672. [[CrossRef](#)]
23. Kouotou, P.M.; Kasmi, A.E.; Wu, L.-N.; Waqas, M.; Tian, Z.-Y. Particle Size-Band Gap Energy-Catalytic Properties Relationship of PSE-CVD-Derived Fe₃O₄ Thin Films. *J. Taiwan Inst. Chem. Eng.* **2018**, *93*, 427–435. [[CrossRef](#)]
24. Li, Z.; Chanéac, C.; Berger, G.; Delaunay, S.; Graff, A.; Lefèvre, G. Mechanism and Kinetics of Magnetite Oxidation under Hydrothermal Conditions. *RSC Adv.* **2019**, *9*, 33633–33642. [[CrossRef](#)] [[PubMed](#)]
25. Kang, M.; Choung, S.-J.; Park, J.Y. Photocatalytic Performance of Nanometer-Sized Fe_xO_y/TiO₂ Particle Synthesized by Hydrothermal Method. *Catal. Today* **2003**, *87*, 87–97. [[CrossRef](#)]
26. Rodríguez, E.; Fernández, G.; Ledesma, B.; Álvarez, P.; Beltrán, F.J. Photocatalytic Degradation of Organics in Water in the Presence of Iron Oxides: Influence of Carboxylic Acids. *Appl. Catal. B Environ.* **2009**, *92*, 240–249. [[CrossRef](#)]
27. Yu, X.; Liu, S.; Yu, J. Superparamagnetic γ-Fe₂O₃@SiO₂@TiO₂ Composite Microspheres with Superior Photocatalytic Properties. *Appl. Catal. B Environ.* **2011**, *104*, 12–20. [[CrossRef](#)]
28. Linnik, O.; Chorna, N.; Smirnova, N.; Eremenko, A.; Korduban, O.; Stefan, N.; Ristoscu, C.; Socol, G.; Miroiu, M.; Mihailescu, I.N. Pulsed Laser-Deposited TiO₂-Based Films: Synthesis, Electronic Structure and Photocatalytic Activity. In *Semiconductor Photocatalysis-Materials, Mechanisms and Applications*; Cao, W., Ed.; InTech: London, UK, 2016; ISBN 978-953-51-2484-9.
29. Linnik, O.; Popescu-Pelin, G.; Stefan, N.; Chorna, N.; Smirnova, N.; Mihailescu, C.N.; Ristoscu, C.; Mihailescu, I.N. Investigation of Nitrogen and Iron Co-Doped TiO₂ Films Synthesized in N₂/CH₄ via Pulsed Laser Deposition Technique. *Appl. Nanosci.* **2020**, *10*, 2569–2579. [[CrossRef](#)]
30. Mercyrani, B.; Hernandez-Maya, R.; Solís-López, M. Photocatalytic Degradation of Orange G Using TiO₂/Fe₃O₄ Nanocomposites. *J. Mater. Sci. Mater. Electron.* **2018**, *29*, 15436–15444. [[CrossRef](#)]
31. Alvarez, P.M.; Jaramillo, J.; López-Piñero, F.; Plucinski, P.K. Preparation and Characterization of Magnetic TiO₂ Nanoparticles and Their Utilization for the Degradation of Emerging Pollutants in Water. *Appl. Catal. B Environ.* **2010**, *100*, 338–345. [[CrossRef](#)]
32. Lei, L.; Aoyama, I. Effect-Directed Investigation and Interactive Effect of Organic Toxicants in Landfill Leachates Combining Microtox Test with RP-HPLC Fractionation and GC/MS Analysis. *Ecotoxicology* **2010**, *19*, 1268–1276. [[CrossRef](#)]